

Stellar chromospheric activity and age relation from open clusters in the LAMOST Survey

JIAJUN ZHANG,^{1,2} JINGKUN ZHAO,¹ TERRY D. OSWALT,³ XIANGSONG FANG,^{4,5} GANG ZHAO,^{1,2} XILONG LIANG,^{1,2}
XIANHAO YE,^{1,2} AND JING ZHONG⁶

¹Key Laboratory of Optical Astronomy, National Astronomical Observatories, Chinese Academy of Sciences, Beijing 100012, China.
zjk@nao.cas.cn

²School of Astronomy and Space Science, University of Chinese Academy of Sciences, Beijing 100049, China

³Embry-Riddle Aeronautical University, 600 S. Clyde Morris Blvd., Daytona Beach FL, USA, 32114. oswaltt1@erau.edu

⁴Chinese Academy of Sciences South America Center for Astronomy, National Astronomical Observatories, CAS, Beijing 100101, China

⁵Instituto de Astronomía, Universidad Católica del Norte, Av. Angamos 0610, Antofagasta, Chile

⁶Key Laboratory for Research in Galaxies and Cosmology, Shanghai Astronomical Observatory, Chinese Academy of Sciences, 80 Nandan Road, Shanghai 200030, China

Submitted to ApJ

ABSTRACT

We identify member stars of more than 90 open clusters in the LAMOST survey. With the method of Fang et al. (2018), the chromospheric activity (CA) indices $\log R'_{\text{CaK}}$ for 1091 member stars in 82 open clusters and $\log R'_{\text{H}\alpha}$ for 1118 member stars in 83 open clusters are calculated. The relations between the average $\log R'_{\text{CaK}}$, $\log R'_{\text{H}\alpha}$ in each open cluster and its age are investigated in different T_{eff} and [Fe/H] ranges. We find that CA starts to decrease slowly from $\log t = 6.70$ to $\log t = 8.50$, and then decreases rapidly until $\log t = 9.53$. The trend becomes clearer for cooler stars. The quadratic functions between $\log R'$ and $\log t$ with $4000\text{K} < T_{\text{eff}} < 5500\text{K}$ are constructed, which can be used to roughly estimate ages of field stars with accuracy about 40% for $\log R'_{\text{CaK}}$ and 60% for $\log R'_{\text{H}\alpha}$.

Keywords: Open star clusters; Stellar ages; Stellar chromospheres

1. INTRODUCTION

As a star ages, stellar rotation slows due to magnetic braking. In response, the magnetic field strength on stellar surface decreases. As the result, chromospheric heating drops. This paradigm is the current explanation for the observed decline in chromospheric activity (CA) with age (Babcock 1961; Charbonneau 2014).

Skumanich (1972) found that CaII HK lines emission decayed as the inverse square root of stellar age. Thus, CA is a potential age indicator. Several efforts have been undertaken to calibrate it. The quantity which is often used to indicate the strength of CA is R'_{HK} . R_{HK} is the ratio of the flux in the core of CaII HK line to bolometric flux (σT_{eff}^4). R_{HK} is converted to R'_{HK} when photospheric contribution is removed. Soderblom et al. (1991) drew a linear relation between age ($\log t$) and CA ($\log R'_{\text{HK}}$) using two open clusters and several visual binaries. They presumed that the relation was deterministic and not just statistical. Later, Rocha-Pinto & Maciel (1998) found a relationship between the observed difference between the stellar isochrone and chromospheric ages, and also the metallicity, as measured by the index [Fe/H] among late-type dwarfs. The chromospheric ages tended to be younger than the isochrone ages for metal-poor stars and the opposite occurred for metal-rich stars. Lachaume et al. (1999) provided a CA vs. age relation for solar-type stars with $B - V > 0.6$ using a piece-wise function. Combining the cluster activity data with modern cluster age estimates, Mamajek & Hillenbrand (2008) derived an improved activity-age calibration for F7-K2 dwarfs with $0.5 \text{ mag} < B - V < 0.9 \text{ mag}$. Pace & Pasquini (2004) used a sample of five open clusters and the sun to study the relation. They found an abrupt decay of CA occurred between 0.6 Gyr and 1.5 Gyr, followed by a very slow decline. Later, Pace (2013) found an L-shaped CA versus age diagram. They suggested the viability of this age

indicator was limited to stars younger than about 1.5 Gyr. They detected no decay of CA after about 2 Gyr. However, [Lorenzo-Oliveira et al. \(2016\)](#) took mass and [Fe/H] biases into account and established the viability of deriving usable chromospheric ages for solar-type stars up to at least 6 Gyr. [Lorenzo-Oliveira et al. \(2018\)](#) found evidence that, for the most homogenous set of old stars, CaII H and K activity indices seemed to continue decreasing after the solar age towards the lower main-sequence. Their results indicated that a significant part of the scatter observed in the age-activity relation of solar twins could be attributed to stellar cycle modulation effects.

The goal of this paper is to investigate the relations between CA and age in different T_{eff} and [Fe/H] ranges using the largest sample of open clusters in LAMOST ([Cui et al. 2012](#); [Zhao et al. 2012](#)). Through these CA-age relations, we hope find a way to roughly estimate ages for main sequence stars in LAMOST, which are difficult to derive using the isochrone method. The paper is organized as follows. Section 2 describes data and sample. The measurements of CA indices $\log R'_{\text{CaK}}$ and $\log R'_{\text{H}\alpha}$ are presented in section 3. Our result and analysis are discussed in section 4. Finally, our main conclusions are summarized in section 5.

2. DATA AND SAMPLE

2.1. An overview of LAMOST

The LAMOST telescope is a special reflecting Schmidt telescope ([Cui et al. 2012](#); [Zhao et al. 2012](#); [Luo et al. 2015](#)). Its primary mirror (Mb) is 6.67m×6.05m and its correcting mirror (Ma) is 5.74m×4.40m. It adopts an innovative active optics technique with 4,000 optical fibers placed on the focal surface. It can obtain spectra of 4,000 celestial objects simultaneously, which makes it the most efficient spectroscope in the world. In 2019 June, the LAMOST official website¹ has released five data releases (DR5_v3) to international astronomers. DR5_v3 has 9,026,365 spectra for 8,183,160 stars, 153,863 galaxies, 52,453 quasars, and 637,889 unknown objects. These spectra cover the wavelength range of 3690-9100Å with a resolution of 1800 at the 5500Å. DR5_v3 also provides stellar parameters such as effective temperature (T_{eff}), metallicity ([Fe/H]), surface gravity ($\log g$) and radial velocity (RV) for millions of stars. The typical error for T_{eff} , [Fe/H], $\log g$ and RV are 110K, 0.19dex, 0.11dex and 4.91 km/s, respectively ([Gao et al. 2015](#)). In this work, we measure CA indices $\log R'_{\text{CaK}}$ and $\log R'_{\text{H}\alpha}$ for the CaII K and H α lines. Our used spectra and stellar parameters including T_{eff} , [Fe/H], $\log g$ and RV are all from DR5_v3.

2.2. Open clusters in LAMOST

[Cantat-Gaudin et al. \(2018\)](#) provided 401,448 member stars with membership probability of 1,229 open clusters in Gaia DR2. We select those member stars with membership probability > 0.6. In addition, Melotte 25 (Hyades) is added from [Röser et al. \(2019\)](#). The celestial coordinates of these member stars are used to cross match with the LAMOST general catalogue. Only dwarfs ($\log g > 4.0$) with 4000K < T_{eff} < 7000K and signal-to-noise ratios (SNRs) satisfied some limits are selected. For a star with multiple spectra, only the spectrum with highest SNR is retained. For the CaII K line, 1,240 spectra of 89 open clusters with SNR g (signal-to-noise ratio in g band) > 30 remain. For the H α line, 1,305 spectra of 93 open clusters with SNR r (signal-to-noise ratio in r band) > 50 remain. Table 1 lists these open clusters. The information about member stars can be found on online materials. The ages of these open clusters are from literatures as shown in Table 1. For most open clusters, their ages are from [Kharchenko et al. \(2013\)](#). However, the ages of eight open clusters are not found in literatures, which are not used to derive CA-age relations. Cluster ages are given as $\log t$, where t is in units of yr. We calculate average [Fe/H] for each open cluster as shown in Table 1.

Table 1. open clusters

name	J2000RA	J2000DEC	$\log t$	References	[Fe/H] _{LA}	[Fe/H] _{stdLA}
NGC.2264	100.217	9.877	6.75	1	0.234	
Collinder.69	83.792	9.813	6.76	1	-0.014	0.1723
IC.348	56.132	32.159	6.78	1	-0.024	0.1755

Table 1 continued on next page

¹ <http://dr5.lamost.org/>

Table 1 (*continued*)

name	J2000RA	J2000DEC	log t	References	[Fe/H] _{LA}	[Fe/H] _{stdLA}
NGC_1333	52.297	31.31	6.8	1	0.196	
ASCC_16	81.198	1.655	7.0	1	-0.102	0.1223
Stock_8	81.956	34.452	7.05	1	-1.189	1.0445
ASCC_21	82.179	3.527	7.11	1	0.053	0.0515
Collinder_359	270.598	3.26	7.45	1	0.034	0.1754
ASCC_19	81.982	-1.987	7.5	1	-0.123	0.088
Stephenson_1	283.568	36.899	7.52	1	0.2	0.0565
NGC_1960	84.084	34.135	7.565	1	-0.246	0.0853
Alessi_20	2.593	58.742	7.575	1	0.057	0.1974
Dolidze_16	78.623	32.707	7.6	1	-0.012	0.036
IC_4665	266.554	5.615	7.63	1	0.09	0.0831
Melotte_20	51.617	48.975	7.7	1	0.041	0.1049
NGC_2232	96.888	-4.749	7.7	1	0.019	0.1087
ASCC_13	78.255	44.417	7.71	1	-0.086	
ASCC_114	324.99	53.997	7.75	1	-0.127	
ASCC_6	26.846	57.722	7.8	1	-0.039	
FSR_0904	91.774	19.021	7.8	1	-0.178	0.0585
Alessi_19	274.741	12.311	7.9	1	0.073	0.0512
ASCC_105	295.548	27.366	7.91	1	0.059	0.0405
Trumpler_2	39.232	55.905	7.925	1	-0.027	0.0365
ASCC_113	317.933	38.638	7.93	1	-0.011	
NGC_7063	321.122	36.507	7.955	1	-0.093	0.0064
NGC_7243	333.788	49.83	7.965	1	-0.068	5.0E-4
ASCC_29	103.571	-1.67	8.06	1	-0.234	0.008
NGC_7086	322.624	51.593	8.065	1	0.004	
Alessi_37	341.961	46.342	8.125	2	0.057	0.0213
Melotte_22	56.601	24.114	8.15	1	0.006	0.1241
Alessi_Teutsch_11	304.127	52.051	8.179	2	0.029	
NGC_2186	93.031	5.453	8.2	1	-0.233	
NGC_2168	92.272	24.336	8.255	1	-0.062	0.0759
Gulliver_20	273.736	11.082	8.289	2	-0.097	0.013
FSR_0905	98.442	22.312	8.3	1	-0.154	
NGC_1647	71.481	19.079	8.3	1	0.025	0.0718
ASCC_11	53.056	44.856	8.345	1	-0.081	0.037
NGC_1912	82.167	35.824	8.35	1	-0.162	0.0342
NGC_2301	102.943	0.465	8.35	1	-0.02	0.0675
NGC_744	29.652	55.473	8.375	1	-0.213	
NGC_1039	40.531	42.722	8.383	1	-0.027	0.1309
Stock_10	84.808	37.85	8.42	1	-0.09	0.0736
ASCC_108	298.306	39.349	8.425	1	-0.046	0.0589
Stock_2	33.856	59.522	8.44	1	-0.056	0.0694

Table 1 continued on next page

Table 1 (*continued*)

name	J2000RA	J2000DEC	log t	References	[Fe/H] _{LA}	[Fe/H] _{stdLA}
Czernik_23	87.525	28.898	8.48	1	0.157	
ASCC.23	95.047	46.71	8.485	1	-0.032	0.074
FSR_0985	92.953	7.02	8.5	1	0.056	
Stock_1	294.146	25.163	8.54	1	0.048	
NGC.1528	63.878	51.218	8.55	1	-0.145	0.0415
NGC.2099	88.074	32.545	8.55	1	-0.017	0.0549
Ferrero_11	93.646	0.637	8.554	2	-0.103	0.044
NGC.7092	322.889	48.247	8.569	1	-0.29	
NGC.1342	52.894	37.38	8.6	1	-0.155	0.0809
NGC.1907	82.033	35.33	8.6	1	-0.18	
NGC.2184	91.69	-2.0	8.6	1	-0.074	0.082
NGC.1750	75.926	23.695	8.617	2	-0.017	0.0846
ASCC.12	72.4	41.744	8.63	1	-0.085	
NGC.6866	300.983	44.158	8.64	1	0.019	0.067
NGC.1582	67.985	43.718	8.665	1	-0.072	0.0742
Roslund_6	307.185	39.798	8.67	1	0.024	0.0797
NGC.1662	72.198	10.882	8.695	1	-0.111	0.0865
Alessi_2	71.602	55.199	8.698	1	-0.01	0.0618
ASCC.41	116.674	0.137	8.7	1	-0.093	0.0774
Collinder_350	267.018	1.525	8.71	1	-0.034	0.0923
ASCC.10	51.87	34.981	8.717	1	-0.02	0.049
NGC.2548	123.412	-5.726	8.72	1	-0.026	0.0624
NGC.1758	76.175	23.813	8.741	2	-0.013	0.0523
NGC.1664	72.763	43.676	8.75	1	-0.082	0.0602
NGC.1708	75.871	52.851	8.755	1	-0.065	0.0236
NGC.6633	276.845	6.615	8.76	1	-0.098	0.0373
NGC.2281	102.091	41.06	8.785	1	-0.033	0.1
IC.4756	279.649	5.435	8.79	1	-0.087	0.0803
NGC.2194	93.44	12.813	8.8	1	-0.008	
NGC.1545	65.202	50.221	8.81	1	-0.001	
Dolidze_8	306.129	42.3	8.855	1	0.025	
Melotte_25	66.725	15.87	8.87	3	-0.003	0.13
NGC.1817	78.139	16.696	8.9	1	-0.205	0.0936
NGC.2355	109.247	13.772	8.9	1	-0.248	0.0538
NGC.2632	130.054	19.621	8.92	1	0.187	0.1053
King_6	51.982	56.444	8.975	1	-0.055	
NGC.6811	294.34	46.378	9.0	4	-0.08	0.0768
NGC.1245	48.691	47.235	9.025	1	-0.186	
NGC.752	29.223	37.794	9.13	1	-0.067	0.0825
Koposov_63	92.499	24.567	9.22	1	-0.016	
NGC.7789	-0.666	56.726	9.265	1	-0.145	0.1199

Table 1 continued on next page

Table 1 (*continued*)

name	J2000RA	J2000DEC	log t	References	[Fe/H] _{LA}	[Fe/H] _{stdLA}
NGC.2112	88.452	0.403	9.315	1	-0.138	0.0311
NGC.2420	114.602	21.575	9.365	1	-0.278	0.0462
NGC.2682	132.846	11.814	9.535	1	-0.003	0.0566
Gulliver_22	84.848	26.368			-0.225	
Gulliver_25	52.011	45.152			-0.009	
Gulliver_6	83.278	-1.652			-0.049	0.1697
Gulliver_60	303.436	29.672			-0.12	0.002
Gulliver_8	80.56	33.792			-0.266	0.0745
RSG_1	75.508	37.475			-0.014	0.0834
RSG_5	303.482	45.574			0.098	0.093
RSG_7	344.19	59.363			0.014	0.012

NOTE—The first column is name of open clusters. The second and third columns are mean right ascension and declination (J2000) of member stars and they are in units of ($^{\circ}$). Mean right ascension and declination of all clusters but Melotte 25 are from [Cantat-Gaudin et al. \(2018\)](#), while the coordinates of Melotte 25 are from [Dias et al. \(2014\)](#). The fourth column is ages of clusters which are represented by $\log t$, where t is in units of yr. The fifth column is references from which the ages are cited: 1-Kharchenko et al. (2013), 2-D. Bossini et al. (2019), 3-Gossage et al. (2018), 4-Sandquist et al. (2016). However, the ages of eight open clusters are not found in literatures. The sixth and seventh columns are the mean value and standard deviation of [Fe/H] of each open cluster. Some clusters have no standard deviation, which means they are represented by only one member star. Note that Stock 8 has [Fe/H]_{LA} = -1.189 . The cluster has only two member stars, of which one has [Fe/H] = -2.23 . This star shouldn't be a member star of the cluster. We don't calculate its $\log R'$ values.

3. DETERMINATION OF EXCESS FRACTIONAL LUMINOSITY

Fang's method ([Fang et al. 2018](#)) is used to calculate the excess fractional luminosities $\log R'_{\text{CaK}}$ for the CaII K line and $\log R'_{\text{H}\alpha}$ for the H α line. We use only the CaII K line because the CaII H line might be polluted by a hydrogen line. First, equivalent width (EW) for the CaII K line and the H α line are measured. Then, excess equivalent width (EW') are obtained. As a last step, we calculate χ , the ratio of the surface continuum flux near the line to the stellar surface bolometric flux from model spectra. We then compute the excess fractional luminosity $\log R'$.

3.1. Measurement of equivalent width

$$\text{EW} = \int \frac{f(\lambda) - f(\lambda_c)}{f(\lambda_c)} d\lambda \quad (1)$$

As an example, the EW of CaII K line is measured by using Equation 1. Here, $f(\lambda_c)$ denotes the pseudo-continuum flux. To measure the EW of the CaII K line, we integrate the line flux from 3930.2 \AA to 3937.2 \AA . The pseudo-continuum flux $f(\lambda_c)$ is estimated by interpolating the flux between 3905.0-3920.0 \AA and 3993.5-4008.5 \AA . These values for CaII K and H α can be found in Table 2.

Figure 1 shows the spectra of an active star (dotted line) and an inactive star (solid line). V and R represent wavelengths of violet and red pseudo-continua, respectively. The labels 'CaK' and 'H α ' illustrate the wavelength regimes of CaII K and H α lines, respectively. EW are measured from radial velocity corrected spectra. Figure 2 plots EW_{CaK} vs. T_{eff} and $\text{EW}_{\text{H}\alpha}$ vs. T_{eff} . Color is used to represent for the ages of open clusters.

We use simple Monte Carlo simulation to obtain the error of EW. Detail information can be found in Appendix A. For the CaII K line, the average error of EW_{CaK} is about 0.1 \AA when $T_{\text{eff}} > 5500\text{K}$. The average error of EW_{CaK} is about 0.2 \AA at $T_{\text{eff}} = 4500\text{K}$. For the H α line, the average error of $\text{EW}_{\text{H}\alpha}$ is about 0.04 \AA .

From Figure 2 (a), it is clear that as T_{eff} decreases, EW_{CaK} first decreases and then increases. Figure 2 (b) shows that as T_{eff} decreases $\text{EW}_{\text{H}\alpha}$ increases. As for the two panels, at high T_{eff} range ($T_{\text{eff}} > 6500\text{K}$), member stars of

different age populations mix. As T_{eff} decreases, young member stars tend to have larger EW than old member stars, which conforms to our expectation. The scatter of EW increases as T_{eff} decreases. Most member stars in our sample have $T_{\text{eff}} > 5500\text{K}$.

Table 2. Equivalent width measurements of CaII K and H α

Line	Line bandpass(\AA)	Pseudo-continua(\AA)
CaII K	3930.2-3937.2	3905.0-3920.0, 3993.5-4008.5
H α	6557.0-6569.0	6547.0-6557.0, 6570.0-6580.0

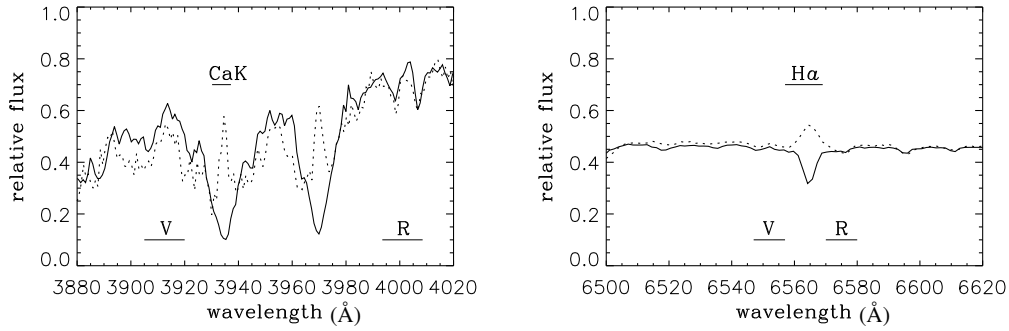


Figure 1. Spectrum of an active star (dotted line) and an inactive star (solid line). The solid lines under the letters indicate the wavelength regimes used to measure EW.

3.2. Excess equivalent width

To measure excess equivalent width EW'_{CaK} and $EW'_{\text{H}\alpha}$, basal lines are needed. The LAMOST official website provides the AFGK type star catalog. In this catalog, stars which satisfy $4000\text{K} < T_{\text{eff}} < 7000\text{K}$, $\log g > 4.0$ and $\text{SNR } g > 30$ ($\text{SNR } r > 50$), the same limitations as member stars, are selected. Further, only stars with $-0.8 < [\text{Fe}/\text{H}] < 0.5$ are selected because at poor $[\text{Fe}/\text{H}]$ range ($[\text{Fe}/\text{H}] \leq -0.8$) there is a negative correlation between EW_{CaK} and $[\text{Fe}/\text{H}]$. We calculate their EW_{CaK} and $EW_{\text{H}\alpha}$ by the same method described in section 3.1. Those stars with $EW > 10\text{\AA}$ or $EW < -10\text{\AA}$ are excluded. Figure 3 shows EW_{CaK} vs. T_{eff} and $EW_{\text{H}\alpha}$ vs. T_{eff} . This plot includes 1,563,898 stars for EW_{CaK} and 1,581,197 stars for $EW_{\text{H}\alpha}$. Few stars are located at about 4570K. This may be caused by a defect in the LAMOST pipeline at this T_{eff} .

Because $[\text{Fe}/\text{H}]$ has more effects on EW_{CaK} than $EW_{\text{H}\alpha}$, we classify stars into three classes according to $[\text{Fe}/\text{H}]$: $-0.8 < [\text{Fe}/\text{H}] < -0.2$, $-0.2 \leq [\text{Fe}/\text{H}] < 0.1$ and $0.1 \leq [\text{Fe}/\text{H}] < 0.5$ before determining the basal lines for EW_{CaK} . For each class, we rebin the stars on T_{eff} with a bin width of 50 K. In each bin, 10% quantile is calculated in EW_{CaK} . Then five order polynomial is fitted to these quantiles as shown in the left panel of Figure 3. The solid lines are fitting curves. From the left panel we can see that the three basal lines corresponding to three different $[\text{Fe}/\text{H}]$ ranges have some differences. When $T_{\text{eff}} > 6000\text{K}$, the basal line of poor $[\text{Fe}/\text{H}]$ range is above on that of rich $[\text{Fe}/\text{H}]$ range. Generally speaking, poor $[\text{Fe}/\text{H}]$ stars have larger EW_{CaK} than rich $[\text{Fe}/\text{H}]$ stars because for poor $[\text{Fe}/\text{H}]$ stars metallic lines are relatively shallow. Note that our EW is negative for an absorption line. For H α , we directly rebin the stars on T_{eff} with a bin width of 50 K without $[\text{Fe}/\text{H}]$ classification and the basal line is obtained by the same method as above. The right panel of Figure 3 shows the basal line for $EW_{\text{H}\alpha}$. Then for member stars, EW'_{CaK} and $EW'_{\text{H}\alpha}$ are obtained by using Equation 2. Stars whose $EW' > 0$ are retained in our study.

$$EW' = EW - EW_{\text{basal}} \quad (2)$$

3.3. Excess fractional luminosity

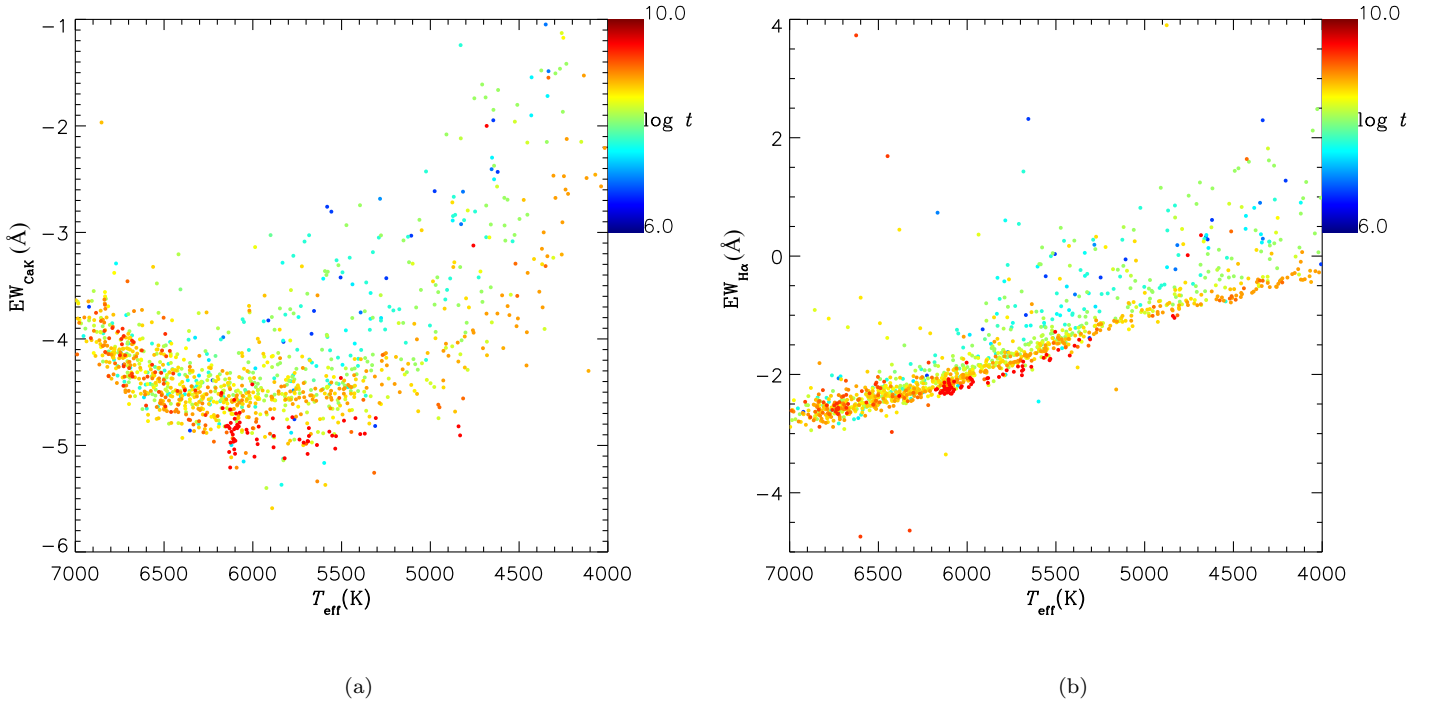


Figure 2. (a): EW_{CaK} vs. T_{eff} . (b): $EW_{\text{H}\alpha}$ vs. T_{eff} . Color is used to represent for the ages of open clusters.

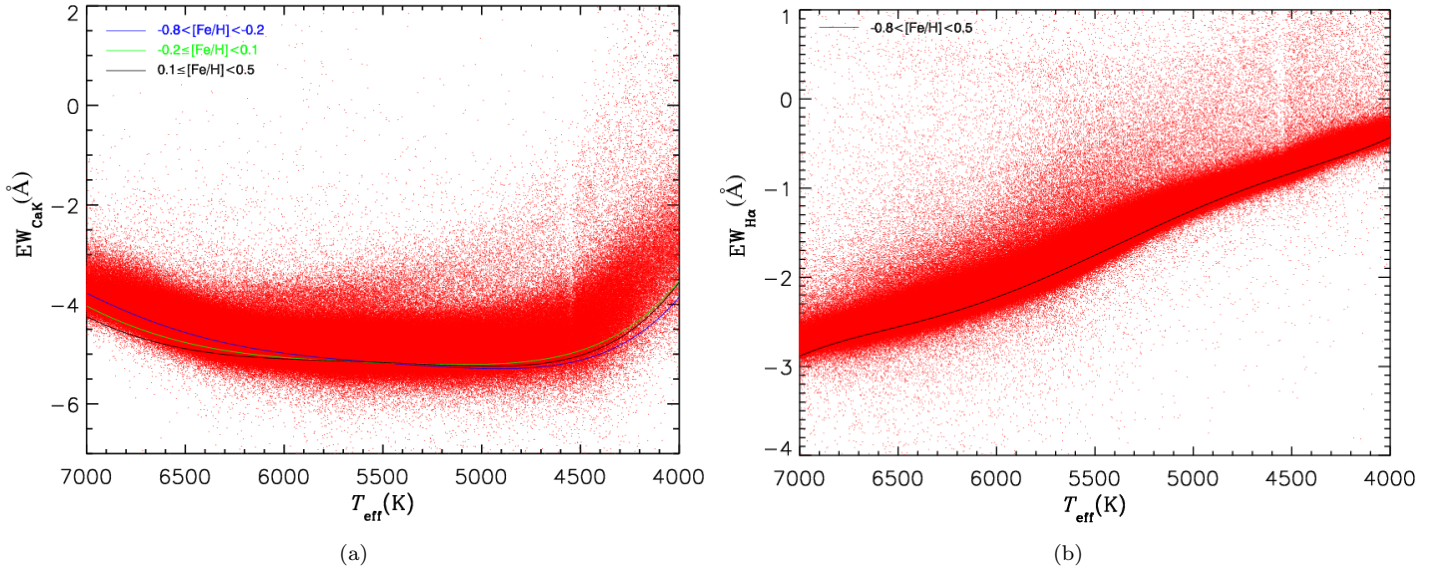


Figure 3. (a): EW_{CaK} vs. T_{eff} for stars in the LAMOST AFGK type star catalog. (b): $EW_{\text{H}\alpha}$ vs. T_{eff} for stars in the same catalog. The scarcity of stars at about 4570K may be caused by a defect in LAMOST pipeline at this T_{eff} . The solid lines in the two panels are our basal lines. The left panel shows three basal lines corresponding to three different $[\text{Fe}/\text{H}]$ ranges.

After obtaining EW' , Equations 3 and 4 are used to calculate the excess fractional luminosity R' . In Equation 3, ATLAS9 model atmospheres² are used to calculate χ of grid points. $F(\lambda)$ is flux at the stellar surface. We choose $\lambda = 3950.5\text{\AA}$ for CaII K and $\lambda = 6560.0\text{\AA}$ for H α . σ is Stefan-Boltzmann constant. Turbulent velocity ($v_{\text{turb}} = 2.0\text{km/s}$) and mixing length parameter ($1/H = 1.25$) are adopted for the model spectra. We calculate χ in terms of T_{eff} , $[\text{Fe}/\text{H}]$ and $\log g$. T_{eff} ranges from 4000K to 7000K in steps of 250K. The values of $\log g$ range from 4.0 to 5.0 in steps of 0.5. $[\text{Fe}/\text{H}]$ ranges from -2.5 to 0.5 in steps of 0.5 plus a value $[\text{Fe}/\text{H}] = 0.2$. Three dimensional linear interpolation is used to obtain the corresponding χ for each star. Finally, excess fractional luminosity R' is obtained by using Equation 4.

$$\chi = \frac{F(\lambda)}{\sigma T_{\text{eff}}^4} \quad (3)$$

$$R' = EW' \times \chi \quad (4)$$

4. RESULTS AND ANALYSIS

4.1. the distribution of $\log R'$

With the above procedures, $\log R'$ value for each member star is obtained. We perform a cross-match between our sample and the Simbad database³, and exclude those stars labeled as 'Flare*', 'pMS*', 'RSCVN', 'SB*', 'EB*WUMa', 'EB*', 'EB*Algol' and 'EB*betLyr' by Simbad. Flare stars and binaries can affect CA level (Curtis 2017; Fang et al. 2018). In Appendix B, we simply discuss the impact of binaries. The result is shown in Figure 4. There are 1091 member stars in 82 open clusters with $\log R'_{\text{CaK}}$ values and 1118 member stars in 83 open clusters with $\log R'_{\text{H}\alpha}$ values. Some open clusters are represented by only one or two stars. The Melotte 22 and NGC 2632 have over 100 member stars. From Figure 4(a) and (b), young member stars have similar $\log R'$ values as old member stars when $T_{\text{eff}} > 6500\text{K}$. As T_{eff} decreases, young member stars tend to have larger $\log R'$ than old member stars, which conforms to our expectation. This phenomena is alike as Figure 2.

We use simple Monte Carlo simulation to obtain the error of $\log R'$. Detail information can be found in Appendix A. For the CaII K line, $\sigma(\log R'_{\text{CaK}})$ has a large scatter when $T_{\text{eff}} > 6000\text{K}$ (see Figure 10). $\sigma(\log R'_{\text{CaK}})$ is about 0.05dex and 0.15dex at 5500K and 4500K. For the H α line, the distribution of $\sigma(\log R'_{\text{H}\alpha})$ has a large scatter from 0.0dex to 0.5dex at all T_{eff} range (see Figure 10).

There are some member stars which should be noticed. In Figure 4(b), we can see that four member stars surrounded by a rectangle box have very high $\log R'_{\text{H}\alpha}$ values, which belong to a same open cluster: NGC 2112 ($\log t = 9.315$). We check their spectra and find that they have very strong balmer emission lines. The open cluster is in the direction of the famous HII region known as Barnard's loop (Haroon et al. 2017). We suspect that the high $\log R'_{\text{H}\alpha}$ values of this cluster are caused by interstellar medium. In (a) and (b) of Figure 4, some member stars have very low values so that they will pull down the mean value of $\log R'$ within an open cluster and increase the scatter obviously. So we exclude those stars whose $\log R'_{\text{CaK}} < -6.40$ for the CaII K line and those stars whose $\log R'_{\text{H}\alpha} < -7.00$ for the H α line.

Mamajek & Hillenbrand (2008) derived CA-age relation by using a traditional indicator $\log R'_{\text{HK}}$ which was derived from S-values in the Mount Wilson HK project (Vaughan et al. 1978; Noyes et al. 1984). We cross match our results with Table 5 of Mamajek & Hillenbrand (2008). The comparison between our results and theirs is shown in Figure 5. The crossing match sample only includes three open clusters: Melotte 20, Melotte 22 and NGC 2682. From Figure 5, as $\log R'_{\text{CaK}}$ or $\log R'_{\text{H}\alpha}$ decreases, $\log R'_{\text{HK}}$ also decreases. However, for those stars whose CA indices are low, our indices show a little larger scatter than theirs, which might be caused by different data processing methods. For stars whose EW are close to the basal lines, their EW' are close to zero and the $\log R'_{\text{CaK}}$ and $\log R'_{\text{H}\alpha}$ values discern more when taking the logarithm. In Appendix C, we list a table (Table 4) to illustrate it.

4.2. $\log R'$ vs. $\log t$

4.2.1. $\log R'$ vs. $\log t$ in different T_{eff} ranges

The mean value of $\log R'_{\text{CaK}}$ ($\log R'_{\text{H}\alpha}$) for each open cluster is calculated. Figure 6 plots this mean value vs. age of each cluster. The left-top corner gives the T_{eff} range of member stars chosen to calculate mean value. Clusters

² wwwuser.oats.inaf.it/castelli/grids.html

³ <http://simbad.u-strasbg.fr/simbad/>

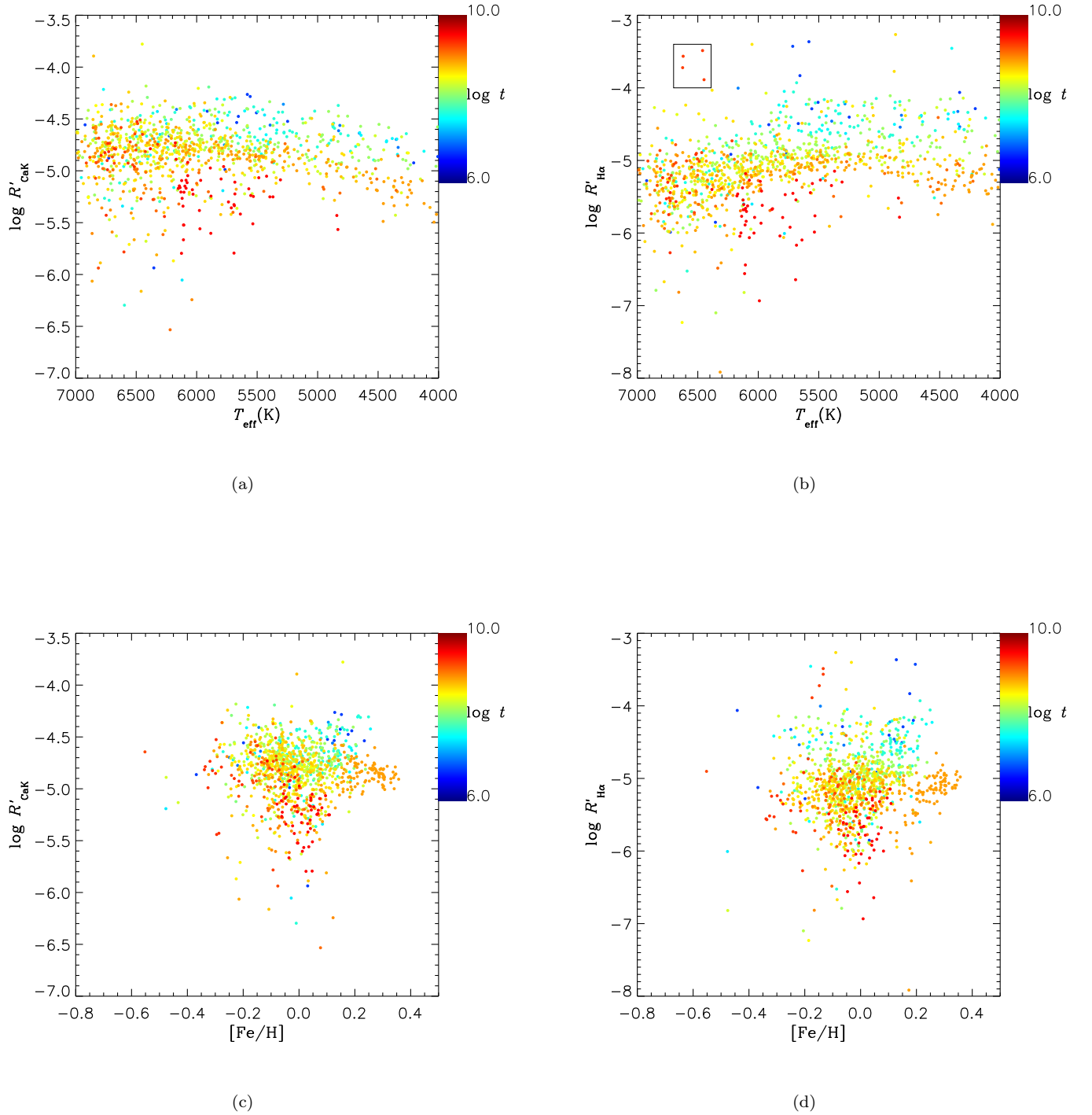


Figure 4. (a): $\log R'_{\text{CaK}}$ vs. T_{eff} . (b): $\log R'_{\text{H}\alpha}$ vs. T_{eff} . (c): $\log R'_{\text{CaK}}$ vs. $[\text{Fe}/\text{H}]$. (d): $\log R'_{\text{H}\alpha}$ vs. $[\text{Fe}/\text{H}]$. The color has the same meaning as Figure 2. This plot includes 1091 member stars of 82 open clusters for CaII K and 1118 member stars of 83 open clusters for H α , respectively.

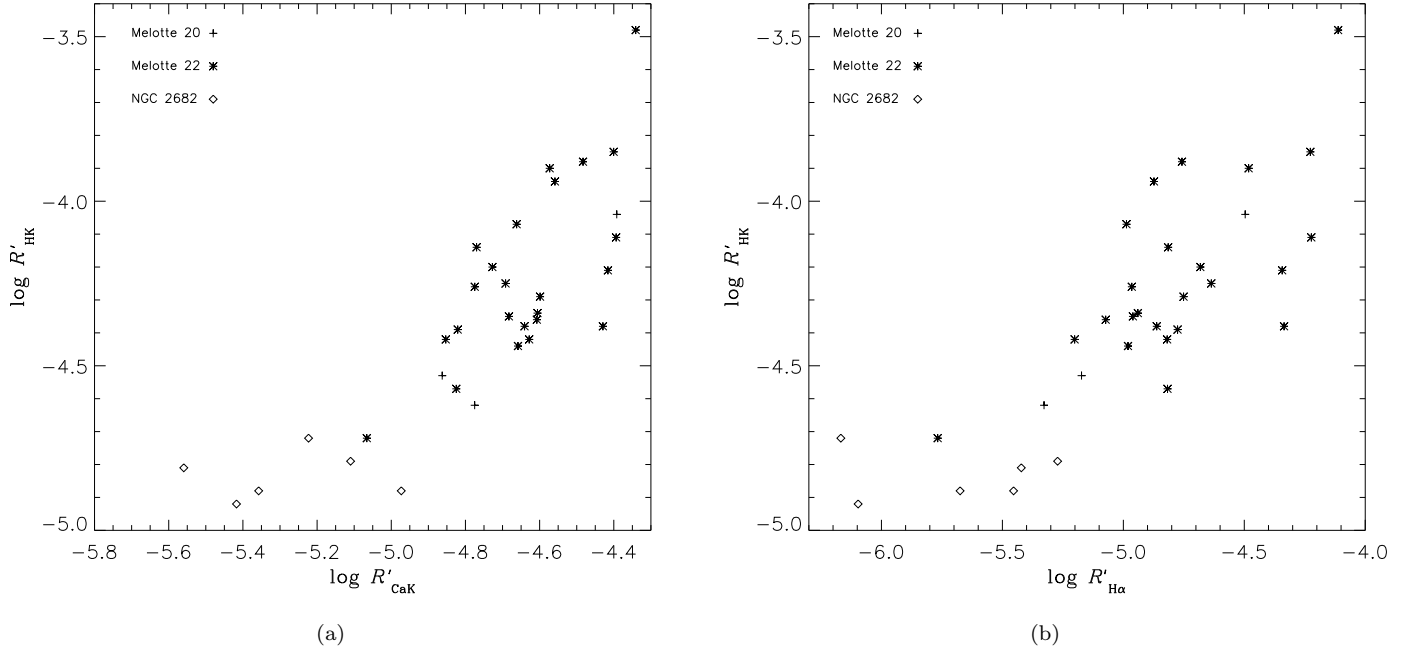


Figure 5. The CA indices comparison for common stars between our sample and those from Mamajek & Hillenbrand (2008), which are member stars in three open clusters: Melotte 20, Melotte 22 and NGC 2682. The $\log R'_{\text{CaK}}$ and $\log R'_{\text{H}\alpha}$ are our CA indices. The $\log R'_{\text{HK}}$ are from Table 5 of Mamajek & Hillenbrand (2008).

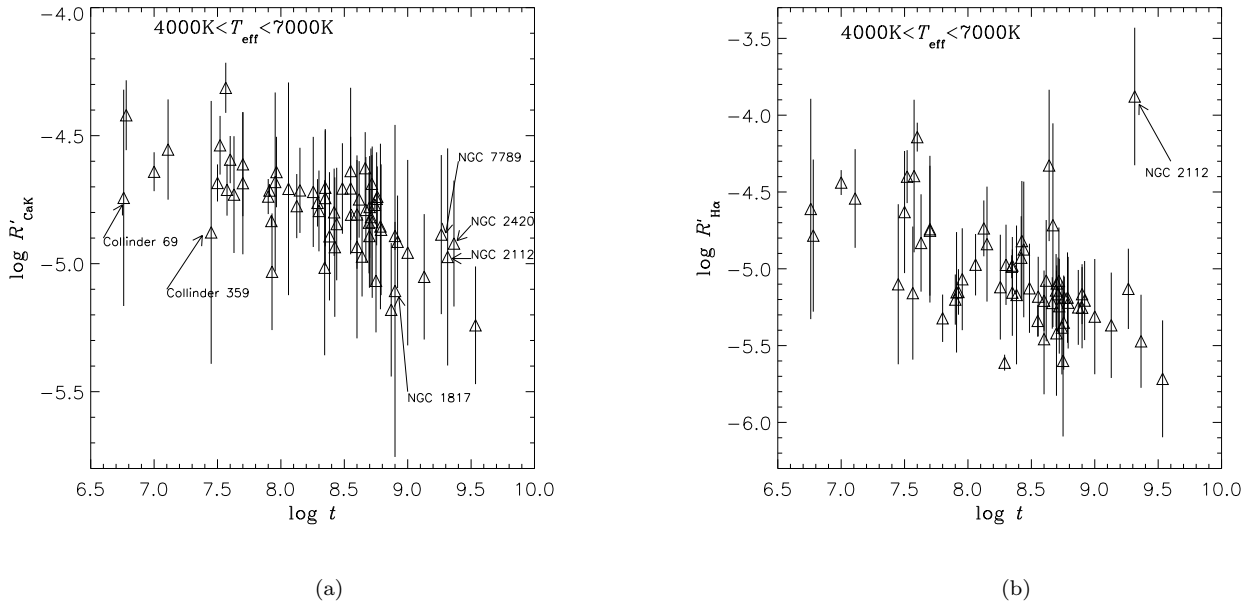


Figure 6. The mean $\log R'$ vs. age $\log t$ among open clusters. Each triangle represents a cluster and error bar indicates the standard deviation of the CA indices in each open cluster. Left-top corner gives the T_{eff} range of stars chosen to calculate the mean values. Those clusters with only one member star are not displayed. Arrows are used to specify the location of some open clusters.

which have only one star are not displayed in this plot. From Figure 6 (a) we find that when stellar age $\log t < 8.5$ (0.3Gyr), the mean value of $\log R'_{\text{CaK}}$ starts to decrease slowly as age increases. Then after $\log t = 8.5$, the mean value decreases rapidly until $\log t = 9.53$ (3.4Gyr). Soderblom et al. (1991) pointed that the evolution of CA for a low-mass star may be going through three stages: a slow initial decline, a rapid decline at intermediate ages ($\sim 1\text{-}2$ Gyr), and a slow decline for old stars like the sun. Although there are some differences on age ranges of each stage, our conclusion is consistent with that of Soderblom et al. (1991) for the two former stages. In our sample, the number of old open clusters ($\log t > 9.0$) is small and the age is only extended to $\log t = 9.53$, so it's hard to see whether there is a slow decline for old stars like the sun. From Figure 6 (b), the mean value of $\log R'_{\text{H}\alpha}$ decreases from nearly $\log t = 6.76$ (5.7Myr) to $\log t = 9.53$ (3.4Gyr). Although it doesn't show the trend: a slow initial decline and then a rapid decline, we can see the same trend as CaII K if we divide T_{eff} range as done below.

From Figure 6, we can see some open clusters deviate from the location of our expectation or have a large error bar. In panel(a), three old open clusters (NGC 7789, NGC 2112 and NGC 2420) show a little larger mean values. Their average $[\text{Fe}/\text{H}]$ are relatively poor compared to young open clusters. For example, NGC 2420 has average $[\text{Fe}/\text{H}]$ equal to -0.278 ± 0.0462 (see Table 1). Poor $[\text{Fe}/\text{H}]$ stars have relatively shallower metallic lines than rich $[\text{Fe}/\text{H}]$ stars, leading to large EW_{CaK} and $\log R'_{\text{CaK}}$, which may be the reason of these larger mean values. Some open clusters have one or two member stars whose $\log R'_{\text{CaK}}$ values are very low, so that they pull down the mean values, like Collinder 69 and Collinder 359. We see that NGC 1817 has a very large error bar. This cluster has five member stars and all stars are with $T_{\text{eff}} > 6500\text{K}$. Three of them have large $\log R'_{\text{CaK}}$ values, the other two have low $\log R'_{\text{CaK}}$ values. The difference between the two groups is about 1 dex. In panel(b), NGC 2112 has a very large mean value. The reason is discussed above.

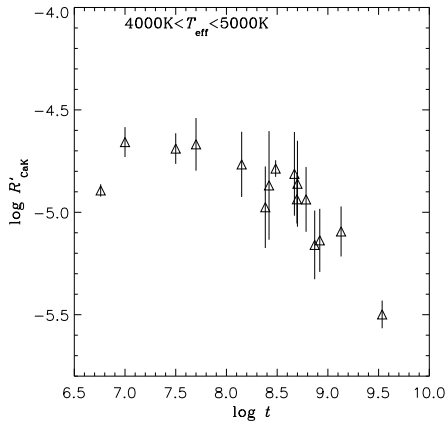
The scatter of $\log R'$ within an open cluster is large. In addition to measurement error, there are many other physical factors contributed to the scatter. Within an open cluster, different member star has different mass and rotation rate. Stellar mass and rotation rate can influence CA level (Noyes et al. 1984; Mamajek & Hillenbrand 2008). Stellar cycle modulations also change CA level (Baliunas et al. 1995; Lorenzo-Oliveira et al. 2018). Some stars in our sample may have flare or starspots, which affect CA level. Binaries and interstellar medium can also influence CA level. Appendix B simply discusses the impact of binaries and interstellar medium on $\log R'$. In our sample, some stars may not belong to open clusters and they affect the mean values. Besides, our data processing method also contributes to the scatter. For those stars whose EW are very close to the basal line, a small difference in EW between two stars can cause a large difference in $\log R'$ (see Table 4).

In order to decrease the influence of stellar mass on CA, we divide T_{eff} into three equal bins and plot the mean $\log R'$ vs. age $\log t$ again as shown in Figure 7. In all T_{eff} ranges, we can see the trend that as age increases the mean value decreases slowly or remains unchanged, and then decreases rapidly. The scatter is smaller at low T_{eff} range than at high T_{eff} range. That means $\log R'$ is more sensitive to stellar age at lower T_{eff} , which is consistent with Figure 2 of Zhao et al. (2011). In their figure, the quantity $\log S_{\text{HK}}$ used to indicate CA level discerned more from each other at redder color. The trend that CA shows a slow decline and then a rapid decline is more evident for cooler stars. This phenomena may be related to stellar inner structure. Those stars at low T_{eff} range have thicker convective zone than those at high T_{eff} range. So those stars at low T_{eff} range can maintain strong surface magnetic field at longer time scale than at high T_{eff} range (Fang et al. 2018; West et al. 2008).

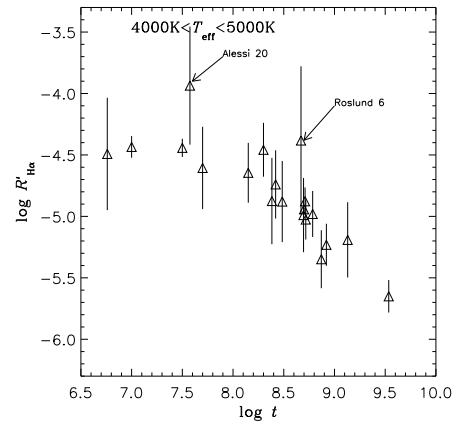
There are some open clusters which deviate from locations of expectation or have a large error bar. Many of them are discussed above. In Figure 7(c), Melotte 25 has a low mean value and a large error bar. The reason is that this cluster has only three member stars at $6000\text{K} < T_{\text{eff}} < 7000\text{K}$, of which one member star has a low $\log R'_{\text{CaK}}$ value ($\log R'_{\text{CaK}} = -5.81$), pulling down the mean value. In Figure 7(d), Alessi 20 has a larger mean value. With $4000\text{K} < T_{\text{eff}} < 5000\text{K}$, this open cluster has only two member stars, whose $[\text{Fe}/\text{H}]$ are poorer compared to the other member stars. One of these two stars shows very strong $\text{H}\alpha$ emission line. Maybe these two stars are not member stars of the cluster. Roslund 6 has only two member stars with $4000\text{K} < T_{\text{eff}} < 5000\text{K}$. The $\text{EW}_{\text{H}\alpha}$ of these two stars are very large. One is 15.13\AA , the other is 3.90\AA . Their spectra show very strong $\text{H}\alpha$ emission line. Not just $\text{H}\alpha$, there are other emission lines in these two spectra such as: $\text{H}\beta$, CaII HK, NII and so on. Maybe the two stars are in a special term. For example, they have large spots on stellar surface.

4.2.2. $\log R'$ vs. $\log t$ in a narrow $[\text{Fe}/\text{H}]$ range

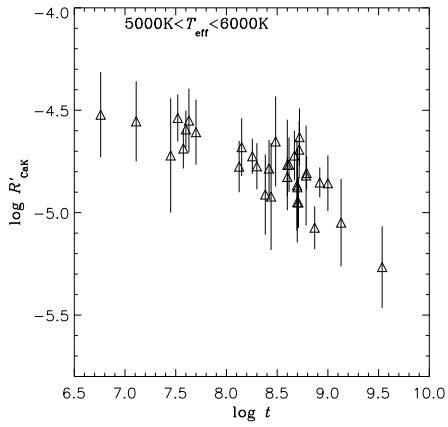
$[\text{Fe}/\text{H}]$ has more effect on $\log R'_{\text{CaK}}$ than $\log R'_{\text{H}\alpha}$ (Rocha-Pinto & Maciel 1998; Rocha-Pinto et al. 2000; Lorenzo-Oliveira et al. 2016). Maybe there is a negative correlation between $\log R'_{\text{CaK}}$ and $[\text{Fe}/\text{H}]$. We narrow $[\text{Fe}/\text{H}]$ range to



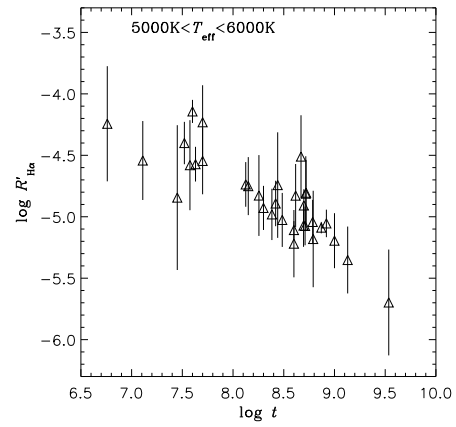
(a)



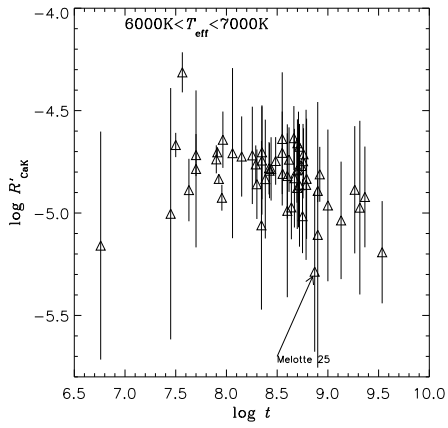
(d)



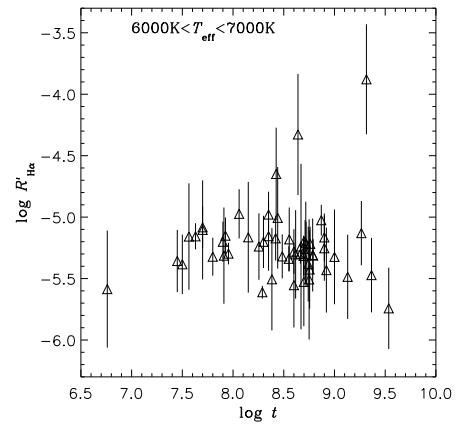
(b)



(e)



(c)



(f)

Figure 7. The mean $\log R'$ vs. age ($\log t$) among open clusters in different T_{eff} ranges. Arrows are used to specify the location of some open clusters.

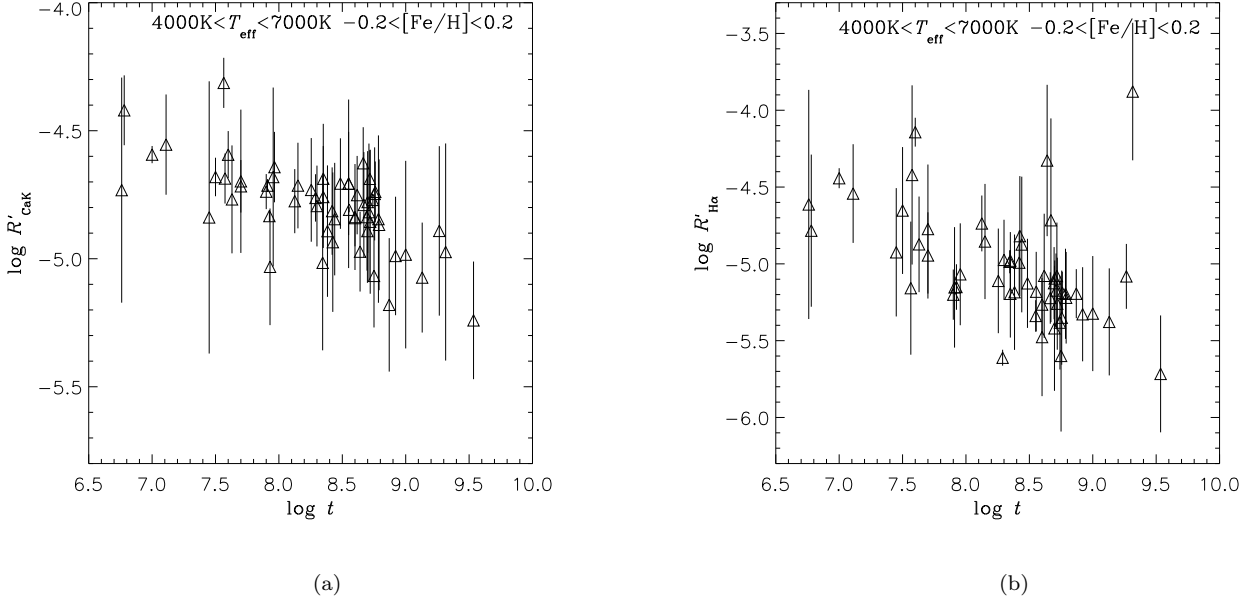


Figure 8. The mean $\log R'$ vs. age ($\log t$) among open clusters with $4000\text{K} < T_{\text{eff}} < 7000\text{K}$ and $-0.2 < [\text{Fe}/\text{H}] < 0.2$.

$-0.2 < [\text{Fe}/\text{H}] < 0.2$ and plot the mean $\log R'$ vs. age $\log t$ again. The sample is split on a star-by-star basis. Figure 8 shows $\log R'$ vs. $\log t$ with $4000\text{K} < T_{\text{eff}} < 7000\text{K}$ and $-0.2 < [\text{Fe}/\text{H}] < 0.2$. By comparing Figure 8 and Figure 6, we find that there is no obvious difference. Figure 9(a) and (c) shows $\log R'$ vs. $\log t$ with $4000\text{K} < T_{\text{eff}} < 5500\text{K}$ and without $[\text{Fe}/\text{H}]$ limit. Figure 9(b) and (d) shows $\log R'$ vs. $\log t$ with $4000\text{K} < T_{\text{eff}} < 5500\text{K}$ and $-0.2 < [\text{Fe}/\text{H}] < 0.2$. By comparison, no obvious difference is formed. We also see no large difference of $\log R'$ vs. $\log t$ relation when narrowing $[\text{Fe}/\text{H}]$ range to $-0.1 < [\text{Fe}/\text{H}] < 0.1$.

4.3. fitting between $\log R'$ and $\log t$ at low T_{eff} range

Quadratic function is used to fit data points with $4000\text{K} < T_{\text{eff}} < 5500\text{K}$ in two $[\text{Fe}/\text{H}]$ ranges. Figure 9 shows fitting curves and relationships. For $\text{H}\alpha$, two stars of Alessi 20 and two stars of Roslund 6 mentioned in 4.2.1 are removed. The relationships are also listed in Equations 5-8. Age for field stars can be approximately estimated by solving these quadratic equations. Via Monte Carlo simulation, a distribution of $\log t$ can be obtained with a $\log R'$ value and its error. For Equations 5 and 6, we calculate two distribution of $\log t$ at two $\log R'_{\text{CaK}}$ values ($\log R'_{\text{CaK}} = -4.90, -5.23$). The error of $\log R'_{\text{CaK}}$ is set to 0.15dex. The error of $\log t$ are about 0.40dex, 0.28dex at $\log t = 8.75, 9.44$ corresponding to $\log R'_{\text{CaK}} = -4.90, -5.23$. The error of $\log t$ at $\log t = 9.44$ is smaller than at $\log t = 8.75$. This is because the fitting curve gets steeper when $\log t$ increases and $\log R'_{\text{CaK}}$ is projected to a smaller range of $\log t$. For Equations 7 and 8, the error of $\log t$ are about 0.40dex, 0.28dex at $\log t = 8.60, 9.40$ corresponding to $\log R'_{\text{H}\alpha} = -4.90, -5.40$. The error of $\log R'_{\text{H}\alpha}$ is set to 0.20dex.

Equations 5 and 7 are used to estimate ages of corresponding clusters whose $\log t > 8.00$. The results and relative error are shown in Table 3. The accuracy of Equation 5 is about 40%, while the accuracy of Equation 7 is about 60%. The ages of NGC 1647 and Ascc 10 can't be estimated by Equation 5 because the two clusters have very large $\log R'_{\text{CaK}}$ mean values which exceed the maximum value of Equation 5.

Equation 5 and Equation 7 are also used to estimate ages of open clusters whose ages are not found in literatures. However, only the open cluster RSG 1 is available to estimate age. The cluster has $\log t = 8.69$ estimated by Equation 5 and $\log t = 8.52$ estimated by Equation 7. In a following paper, we will use Equations 5-8 to roughly estimate ages of field stars.

$$\log R'_{\text{CaK}} = -12.45 + 2.10 \log t - 0.14(\log t)^2, \quad (5)$$

$$\log R'_{\text{CaK}} = -11.22 + 1.82 \log t - 0.13(\log t)^2, \quad -0.2 < [\text{Fe}/\text{H}] < 0.2 \quad (6)$$

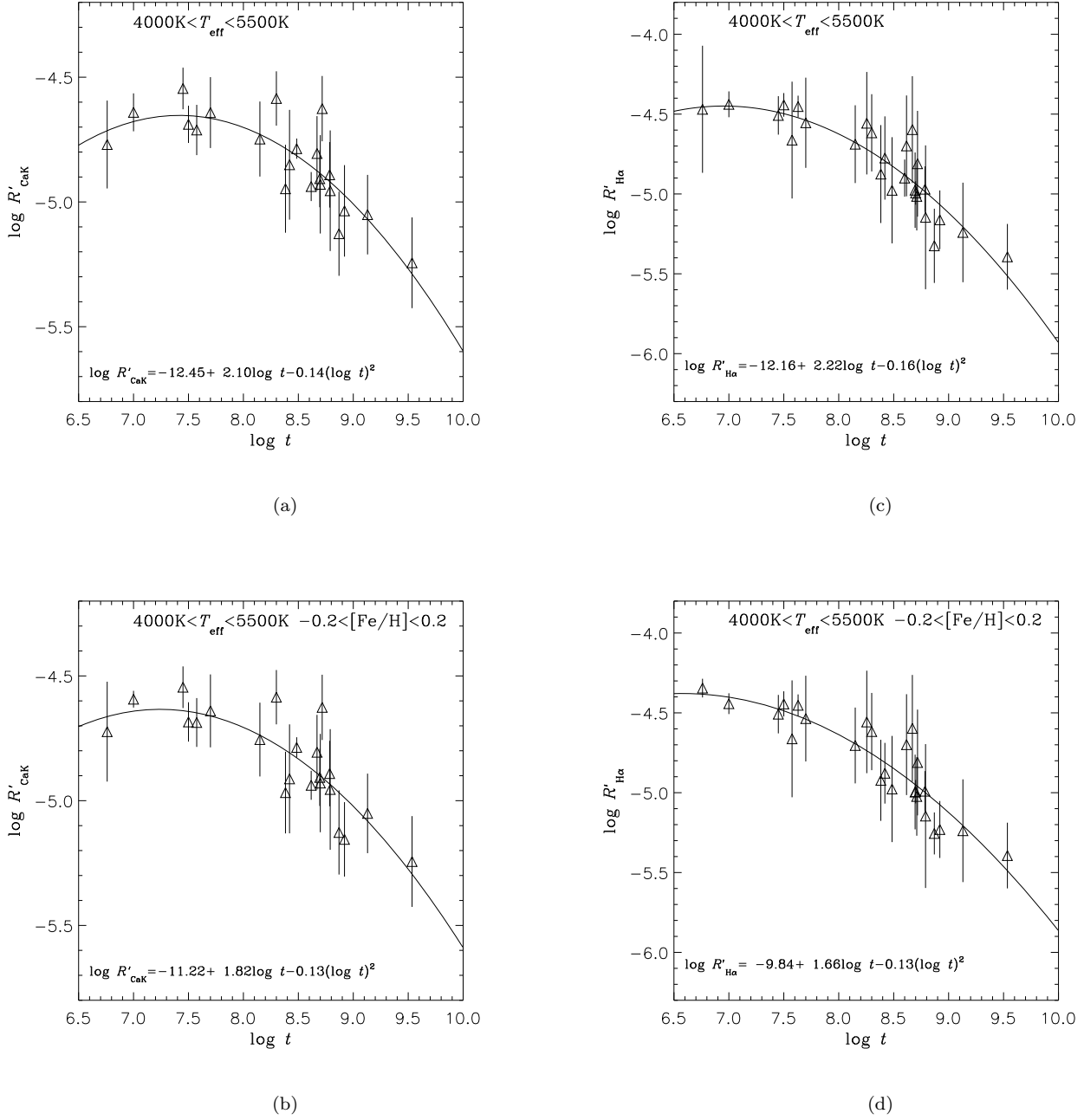


Figure 9. The mean $\log R'$ vs. age ($\log t$) with $4000\text{K} < T_{\text{eff}} < 5500\text{K}$ in two $[\text{Fe}/\text{H}]$ ranges. Quadratic function is used to fit these data points. Relationship is listed in the left-bottom corner. For $\text{H}\alpha$, two stars of Alessi 20 and two stars of Roslund 6 mentioned in 4.2.1 are removed.

$$\log R'_{\text{H}\alpha} = -12.16 + 2.22 \log t - 0.16(\log t)^2, \quad (7)$$

$$\log R'_{\text{H}\alpha} = -9.84 + 1.66 \log t - 0.13(\log t)^2, -0.2 < [\text{Fe}/\text{H}] < 0.2 \quad (8)$$

Table 3. Estimated ages of corresponding open clusters whose $\log t > 8.00$

name	t	Equation 5	relative error	Equation 7	relative error
	Myr	Myr		Myr	
Melotte_22	141	176	25%	147	4%
NGC_2168	180			58	68%
NGC_1647	200			93	53%
NGC_1039	242	732	203%	380	57%
Stock_10	263	405	54%	237	10%
ASCC_23	305	249	19%	582	91%
NGC_1342	398			424	6%
NGC_1750	414	696	68%	157	62%
Roslund_6	468	292	38%	80	83%
NGC_1662	495	580	17%	580	17%
ASCC_41	501	661	32%	623	24%
Collinder_350	513			676	32%
ASCC_10	521			283	46%
NGC_2281	610	526	14%	566	7%
IC_4756	617	766	24%	1088	76%
Melotte_25	741	1788	141%	1950	163%
NGC_2632	832	1169	41%	1150	38%
NGC_752	1349	1258	7%	1495	11%
NGC_2682	3428	2918	15%	2403	30%

NOTE—The first column is the names of open clusters. The second column is the ages (t) of clusters from references. The third and fourth columns are the estimated ages from Equation 5 and its relative error. The fifth and sixth columns are the estimated ages from Equation 7 and its relative error.

5. CONCLUSION AND OUTLOOK

In this paper, we investigate the CA-age relationship by using the largest sample of open clusters in the LAMOST survey. Fang’s method (Fang et al. 2018) is used to calculate excess fractional luminosity $\log R'_{\text{CaK}}$, $\log R'_{\text{H}\alpha}$ of every member star which can be used to indicate CA level. In this method, we use 10% quantile in EW to obtain the basal lines. Excess equivalent width EW' can be obtained after subtracting EW_{basal} . Then R' can be obtained via $R' = \text{EW}' \times \chi$, of which χ is the ratio of the surface continuum flux near the line to the stellar surface bolometric flux from model spectra.

For each open cluster, the average $\log R'_{\text{CaK}}$, $\log R'_{\text{H}\alpha}$ can be calculated. For CaII K, 1091 member stars of 82 open clusters have $\log R'_{\text{CaK}}$ measurements. For H α , 1118 member stars of 83 open clusters have $\log R'_{\text{H}\alpha}$ measurements. Then the relationship between the average $\log R'$ and the age can be studied in different T_{eff} ranges and [Fe/H] ranges. We find that CA starts to decrease slowly from $\log t = 6.70$ to $\log t = 8.50$, then decreases rapidly until $\log t = 9.53$, which is consistent with the point of Soderblom et al. (1991). The trend is more evident for cooler stars. This phenomena may be related to stellar inner structure. Compared to stars at high T_{eff} , stars at low T_{eff} have thicker convective zone, such that they can maintain strong surface magnetic field at longer time scale. We narrow [Fe/H] range to $-0.2 < [\text{Fe}/\text{H}] < 0.2$ and find that there is no obvious difference. Finally, we construct quadratic functions between $\log R'$ and $\log t$ with $4000\text{K} < T_{\text{eff}} < 5500\text{K}$, which can be used to roughly estimate ages of field stars with accuracy about 40% for $\log R'_{\text{CaK}}$ and 60% for $\log R'_{\text{H}\alpha}$.

The LAMOST telescope has obtained about 9 million spectra. The relations shown in Equations 5-8 suggest that $\log R'$ can be used to roughly estimate stellar ages for dwarfs. With reliable stellar ages, the evolution of the thin disk

can be investigated. For example, we can study the spatial age distribution and relations between the stellar age and velocity. Older open clusters are needed to extend the CA-age relation. Medium resolution spectra ($R \sim 8000$) being obtained with the ongoing LAMOST survey may improve the CA-age relation in the near future.

This work is supported by the Astronomical Big Data Joint Research Center, co-founded by the National Astronomical Observatories, Chinese Academy of Sciences and the Alibaba Cloud, the National Natural Science Foundation of China under grant No.11973048, 11573035, 11625313, 11890694. Support from the US National Science Foundation (AST-1358787) to Embry-Riddle Aeronautical University is acknowledged. Guoshoujing Telescope (the Large Sky Area Multi-Object Fiber Spectroscopic Telescope LAMOST) is a National Major Scientific Project built by the Chinese Academy of Sciences. Funding for the project has been provided by the National Development and Reform Commission. LAMOST is operated and managed by the National Astronomical Observatories, Chinese Academy of Sciences.

REFERENCES

- Babcock, H. W. 1961, *ApJ*, 133, 572
- Baliunas, S. L., Donahue, R. A., Soon, W. H., et al. 1995, *ApJ*, 438, 269
- D. Bossini, A. Vallenari, A. Bragaglia, et al. 2019, *A&A*, 623, A108
- Cantat-Gaudin, T., Jordi, C., Vallenari, A., et al. 2018, *A&A*, 618, A93
- Charbonneau, P. 2014, *ARA&A*, 52, 251
- Cui, X.-Q., Zhao, Y.-H., Chu, Y.-Q., et al. 2012, *Research in Astronomy and Astrophysics*, 12, 1197
- Curtis, J. L. 2017, *AJ*, 153, 275
- Dias, W. S., Monteiro, H., Caetano, T. C., et al. 2014, *A&A*, 564, A79
- Fang, X.-S., Zhao, G., Zhao, J.-K., & Bharat Kumar, Y. 2018, *MNRAS*, 476, 908
- Gao, H., Zhang, H.-W., Xiang, M.-S., et al. 2015, *Research in Astronomy and Astrophysics*, 15, 2204
- Gossage, S., Conroy, C., Dotter, A., et al. 2018, *ApJ*, 863, 67
- Haroon, A. A., Ismaill, H. A., & Elsanhoury, W. H. 2017, *Astrophysics*, 60, 173
- Kharchenko, N. V., Piskunov, A. E., Schilbach, E., Röser, S., & Scholz, R.-D. 2013, *A&A*, 558, A53
- Lachaume, R., Dominik, C., Lanz, T., & Habing, H. J. 1999, *A&A*, 348, 897
- Lorenzo-Oliveira, D., Porto de Mello, G. F., & Schiavon, R. P. 2016, *A&A*, 594, L3
- Lorenzo-Oliveira, D., Freitas, F. C., Meléndez, J., et al. 2018, *A&A*, 619, A73
- Luo, A.-L., Zhao, Y.-H., Zhao, G., et al. 2015, *Research in Astronomy and Astrophysics*, 15, 1095
- Mamajek, E. E., & Hillenbrand, L. A. 2008, *ApJ*, 687, 1264
- Noyes, R. W., Hartmann, L. W., Baliunas, S. L., Duncan, D. K., & Vaughan, A. H. 1984, *ApJ*, 279, 763
- Pace, G., & Pasquini, L. 2004, *A&A*, 426, 1021
- Pace, G. 2013, *A&A*, 551, L8
- Rocha-Pinto, H. J., & Maciel, W. J. 1998, *MNRAS*, 298, 332
- Rocha-Pinto, H. J., Maciel, W. J., Scalo, J., & Flynn, C. 2000, *A&A*, 358, 850
- Röser, S., Schilbach, E., & Goldman, B. 2019, *A&A*, 621, L2
- Sandquist, E. L., Jessen-Hansen, J., Shetrone, M. D., et al. 2016, *ApJ*, 831, 11
- Skumanich, A. 1972, *ApJ*, 171, 565
- Soderblom, D. R., Duncan, D. K., & Johnson, D. R. H. 1991, *ApJ*, 375, 722
- Vaughan, A. H., Preston, G. W., & Wilson, O. C. 1978, *PASP*, 90, 267
- West, A. A., Hawley, S. L., Bochanski, J. J., et al. 2008, *AJ*, 135, 785
- Zhao, G., Zhao, Y.-H., Chu, Y.-Q., Jing, Y.-P., & Deng, L.-C. 2012, *Research in Astronomy and Astrophysics*, 12, 723
- Zhao, J. K., Oswalt, T. D., Rudkin, M., Zhao, G., & Chen, Y. Q. 2011, *AJ*, 141, 107

APPENDIX

A. MEASUREMENT ERROR OF EW AND $\log R'$

Monte Carlo simulation is used to obtain the error of EW. For a spectrum, flux at every data point has a inverse variance. So the random flux can be produced following a gaussian distribution of μ (flux at a data point) and σ (inverse variance). In our simulation, we produce 1,000 simulated spectra and calculate their EW. The standard deviation of EW is used as the error of EW. Figure 10(a) and (b) plots $\sigma(\text{EW})$ vs. T_{eff} . From Figure 10(a), the error of EW_{CaK} increases slightly as T_{eff} decreases. The average error of EW_{CaK} is about 0.1\AA when $T_{\text{eff}} > 5500\text{K}$ and about 0.2\AA at $T_{\text{eff}} = 4500\text{K}$. From Figure 10(b), we see that the bottom boundary of distribution of $\sigma(\text{EW}_{\text{H}\alpha})$ increases slightly when T_{eff} decreases from 5500K . The average error of $\text{EW}_{\text{H}\alpha}$ is about 0.04\AA .

The error of $\log R'$ is also estimated by using Monte Carlo simulation again. Only four factors are considered: the EW and stellar atmospheric parameters including T_{eff} , $[\text{Fe}/\text{H}]$ and $\log g$. Errors of T_{eff} , $[\text{Fe}/\text{H}]$ and $\log g$ are set to 110K , 0.12 dex and 0.11 dex, respectively. Figure 10(c) and (d) shows $\sigma(\log R')$ vs. T_{eff} . From Figure 10(c), we see that when $T_{\text{eff}} > 6000\text{K}$, $\sigma(\log R'_{\text{CaK}})$ shows a large scatter. The large scatter is mainly due to small EW'_{CaK} which means EW_{CaK} are close to the basal line. If a star has EW_{CaK} close to the basal line, its EW'_{CaK} is close to zero. A small difference in EW_{CaK} can cause a large difference in $\log R'_{\text{CaK}}$ when taking logarithm of R' ($R' = \text{EW}' \times \chi$). When $T_{\text{eff}} < 6000\text{K}$, $\sigma(\log R'_{\text{CaK}})$ shows a relatively tight distribution. The errors are about 0.05 dex and 0.15 dex at 5500K and 4500K . There is no large scatter at this T_{eff} range because as T_{eff} decreases the distribution of EW_{CaK} shows a large scatter (see Figure 2) and many stars have relatively large EW'_{CaK} . From Figure 10(d), we see that at all T_{eff} range $\sigma(\log R'_{\text{H}\alpha})$ shows a very large scatter from 0.0 dex to 0.5 dex. The reason is same as above. However, for the $\text{H}\alpha$, many member stars have $\text{EW}_{\text{H}\alpha}$ close to the basal line not only at high T_{eff} range but also at low T_{eff} range.

B. THE IMPACT OF BINARIES AND INTERSTELLAR MEDIUM ON $\log R'$

The interaction of two stars can affect CA level. The member stars list provided by Cantat-Gaudin et al. (2018) include gaia color ($G_{BP} - G_{RP}$) and visual magnitude (G_{mag}). According to these information, we can plot CMD (color magnitude diagram) of each open cluster. On CMD, some member stars lie above the single main sequence and many of them are binaries. We try to check change of mean value and scatter of $\log R'$ by discarding these stars. For example, after discarding these stars of NGC 2632, the mean value and standard error of $\log R'_{\text{CaK}}$ changes from -5.04 ± 0.184 to -5.05 ± 0.184 with $4000\text{K} < T_{\text{eff}} < 5500\text{K}$. The same value of $\log R'_{\text{H}\alpha}$ changes from -5.16 ± 0.185 to -5.18 ± 0.178 with $4000\text{K} < T_{\text{eff}} < 5500\text{K}$. Note that we do not consider the labels provided by simbad. The change of the mean values is very small.

The interstellar medium (ISM) imprints absorption lines in the vicinity of the CaII H & K line cores, which negatively biases CA indice (Pace & Pasquini 2004; Curtis 2017). Our spectra are low resolution spectra ($R \sim 1800$ at 5500\AA) and they are not much likely to show evident ISM absorption lines at the wavelength of the CaII H & K line. $\text{H}\alpha$ line is less affected by ISM. So we can find some open clusters which are coeval but separated by a large distance. Then we plot the distributions of $\log R'_{\text{CaK}}$ vs. T_{eff} and $\log R'_{\text{H}\alpha}$ vs. T_{eff} . If ISM affect our results, at a similar range of T_{eff} , the $\log R'_{\text{CaK}}$ values of nearby cluster suppose to be higher than that of distant cluster, but the $\log R'_{\text{H}\alpha}$ values should keep consistent. However, in our sample, the number of member stars for some open clusters are small. Besides, many open clusters have most member stars with $T_{\text{eff}} > 6000\text{K}$. When $T_{\text{eff}} > 6000\text{K}$, $\log R'$ values of member stars of different ages can mix. Fortunately, we find two open clusters: NGC 2281 and Melotte 25 (Hyades). NGC 2281 has $\log t = 8.78$ (Kharchenko et al. 2013) and $d = 519\text{pc}$ (Cantat-Gaudin et al. 2018). d is the distance to the sun. Melotte 25 has $\log t = 8.87$ (Gossage et al. 2018) and $d = 48\text{pc}$ (Röser et al. 2019). There is more than 100Myr age difference between the two clusters. The distributions of $\log R'$ vs. T_{eff} are shown in Figure 11. When $T_{\text{eff}} < 6000\text{K}$, NGC 2281 has a little larger $\log R'_{\text{CaK}}$ and $\log R'_{\text{H}\alpha}$ values than that of Melotte 25 at a similar range of T_{eff} , which suggests that the impact of ISM is smaller compared to the decrease in CA over time.

C. AN ILLUSTRATION OF LOGARITHM EFFECT

During data processing, EW of some member stars are close to the basal lines. For those stars, a small difference in EW can cause a large difference in $\log R'$. This is because EW close to the basal line leads to EW' close to zero and R' close to zero ($R' = \text{EW}' \times \chi$), then R' is projected to a large range when taking logarithm. We list some examples in Table 4 to illustrate it.

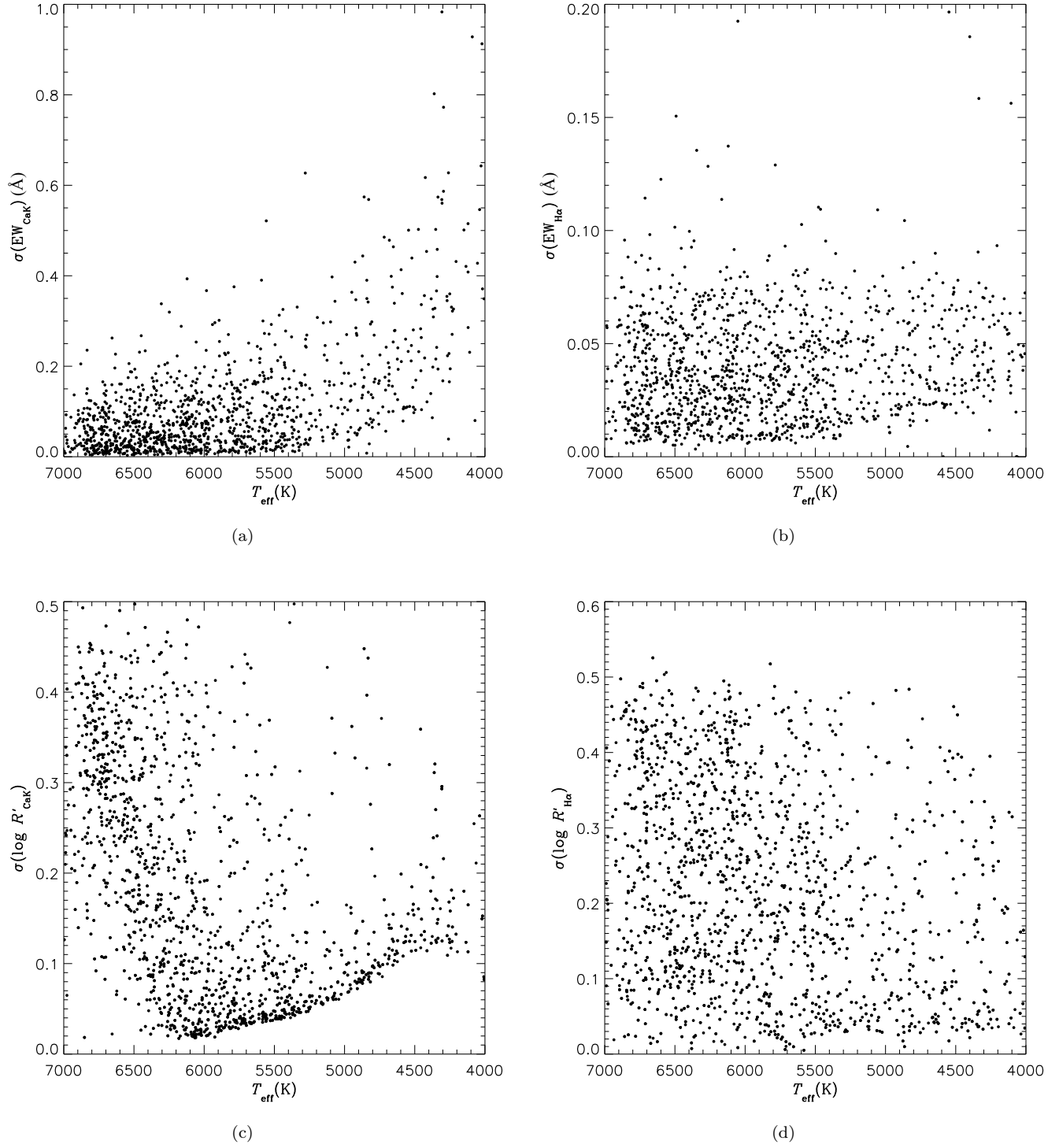


Figure 10. (a): $\sigma(\text{EW}_{\text{CaK}})$ vs. T_{eff} . (b): $\sigma(\text{EW}_{\text{H}\alpha})$ vs. T_{eff} . (c): $\sigma(\log R'_{\text{CaK}})$ vs. T_{eff} . (d): $\sigma(\log R'_{\text{H}\alpha})$ vs. T_{eff} .

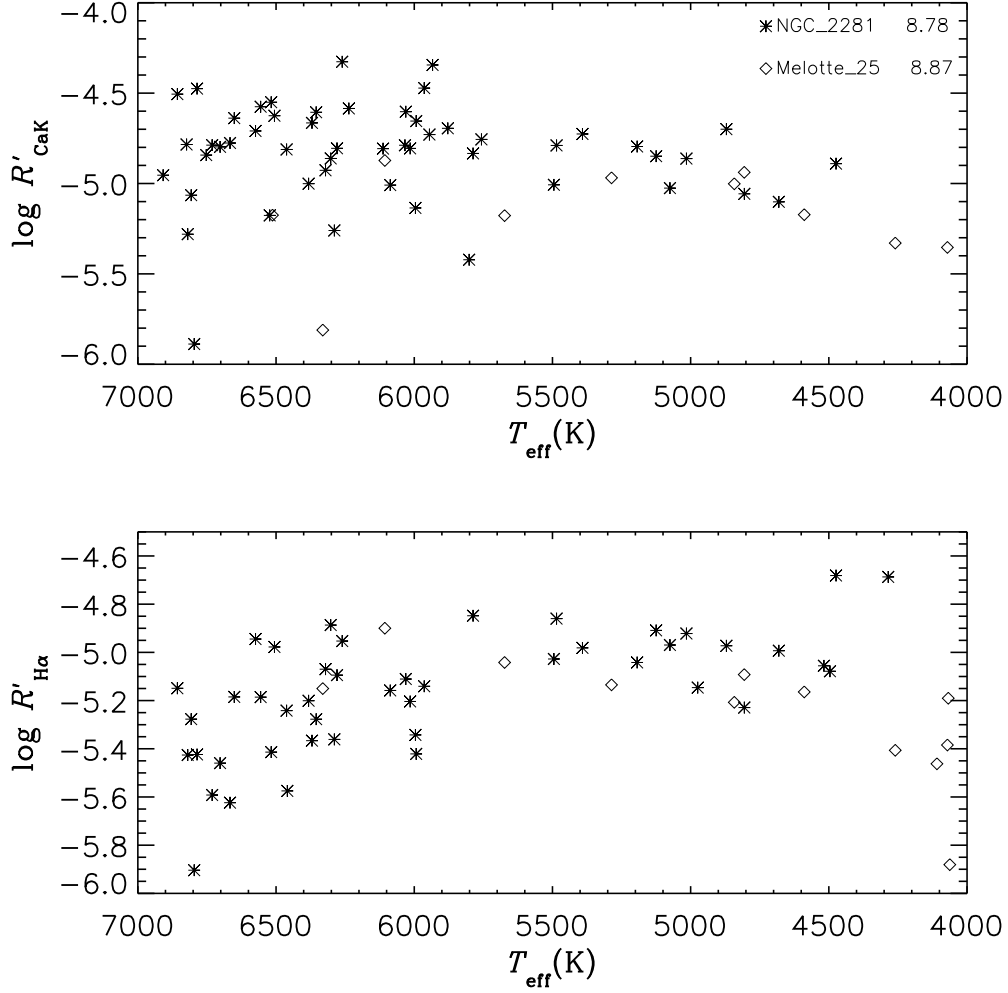


Figure 11. Top panel is $\log R'_{\text{CaK}}$ vs. T_{eff} . Bottom panel is $\log R'_{\text{H}\alpha}$ vs. T_{eff} . The asterisk represents for NGC 2281 while the diamond represents for Melotte 25.

Table 4. Some examples to illustrate logarithm effect

T_{eff} (K)	EW_{CaK} (Å)	$\log R'_{\text{CaK}}$	$\text{EW}_{\text{H}\alpha}$ (Å)	$\log R'_{\text{H}\alpha}$
6500	-4.50	-4.92	-2.50	-5.75
6500	-4.00	-4.46	-2.00	-4.77
6500	-3.50	-4.24	-1.50	-4.49
5500	-5.00	-5.42	-1.70	-5.74
5500	-4.50	-4.83	-1.20	-4.72
5500	-4.00	-4.59	-0.70	-4.44
4500	-4.50	-5.59	-0.70	-5.40
4500	-4.00	-5.25	-0.20	-4.71
4500	-3.50	-5.06	0.30	-4.46

NOTE—Note that $[\text{Fe}/\text{H}]$ and $\log g$ are set to 0.0 and 4.2.